

# Joint Beamforming Design and Bit Allocation in Massive MIMO with Resolution-Adaptive ADCs

Mengyuan Ma, *Student Member, IEEE*, Nhan Thanh Nguyen, *Member, IEEE*,  
Italo Atzeni, *Senior Member, IEEE*, and Markku Juntti, *Fellow, IEEE*

**Abstract**—Low-resolution analog-to-digital converters (ADCs) have emerged as a promising technology for reducing power consumption and complexity in massive multiple-input multiple-output (MIMO) systems while maintaining satisfactory spectral and energy efficiencies (SE/EE). In this work, we first identify the essential properties of optimal quantization and leverage them to derive a closed-form approximation of the covariance matrix of the quantization distortion. The theoretical finding facilitates the system SE analysis in the presence of low-resolution ADCs. We then focus on the joint optimization of the transmit-receive beamforming and bit allocation to maximize the SE under constraints on the transmit power and the total number of active ADC bits. To solve the resulting mixed-integer problem, we first develop an efficient beamforming design for fixed ADC resolutions. Then, we propose a low-complexity heuristic algorithm to iteratively optimize the ADC resolutions and beamforming matrices. Numerical results for a  $64 \times 64$  MIMO system demonstrate that the proposed design offers 6% improvement in both SE and EE with 40% fewer active ADC bits compared with the uniform bit allocation. Furthermore, we numerically show that receiving more data streams with low-resolution ADCs can achieve higher SE and EE compared to receiving fewer data streams with high-resolution ADCs.

**Index Terms**—Beamforming, bit allocation, massive MIMO, low-resolution ADCs, spectral efficiency, energy efficiency

## I. INTRODUCTION

Massive multiple-input multiple-output (MIMO) is a crucial physical-layer technology for wireless communications at both sub-6GHz and millimeter wave (mmWave) frequencies [1], addressing the increasing demand for high data rates [2]. The large number of antenna elements in massive MIMO significantly improves spatial multiplexing gain through beamforming techniques. Digital beamforming (DBF) architectures, which deploy a dedicated radio-frequency (RF) chain for each antenna element, can enable high spectral efficiency (SE) but incur substantial energy costs due to power-intensive RF components, especially analog-to-digital converters (ADCs). For instance, a high-speed ADC operating at 1 Gsample/s with high resolution (e.g., 8–12 bits) can consume several Watts [3]. Furthermore, its power consumption increases linearly with the signal bandwidth and exponentially with the number of resolution bits [4], [5], posing a significant challenge to the system’s energy efficiency (EE). Consequently, the integration of low-resolution ADCs and DBF has emerged as an effective

strategy to curtail power consumption without unduly compromising the SE [6].

Another attractive solution in this regard is to utilize hybrid beamforming (HBF) architectures, where a small number of RF chains is connected to the antenna array through a network of phase shifters or switches [7]–[9]. However, HBF architectures have limited multiplexing capabilities and strongly depend on the calibration of the analog components [10]. Consequently, DBF requires less circuit cost to achieve a SE similar to HBF [11], which makes the former more energy efficient, especially when using low-resolution ADCs [10], [12]. The water-filling (WF) power allocation achieves the capacity of a full-resolution MIMO system with perfect channel state information (CSI) at both the transmitter and receiver [13]. However, it becomes suboptimal in the presence of quantization, necessitating a more efficient design. Furthermore, adopting resolution-adaptive ADCs can enable order-of-magnitude power savings for realistic mmWave channels [14]. These considerations motivate us to focus on the design and analysis of fully digital architectures with resolution-adaptive ADCs.

### A. Prior Works

Recent years have witnessed a proliferation of studies on low-resolution massive MIMO transceivers, exploring various quantization techniques including one-bit, multi-bit, mixed-bit, and variable-bit quantization. One-bit quantized systems have been extensively investigated in the literature due to their simplicity and tractability [3], [15]–[19]. Specifically, Mo *et al.* [16] derived the exact channel capacity with perfect CSI at both the transmitter and receiver of a multi-input single-output system. It was shown in [17] that with only receive CSI, quadrature phase-shift keying (QPSK) signaling is the capacity-achieving distribution in single-input single-output systems, unlike in the full-resolution case where a Gaussian codebook is optimal. At low signal-to-noise ratio (SNR), the mutual information of a one-bit quantized MIMO system decreases by a factor of  $\frac{2}{\pi}$  compared with a full-resolution one [18]. Although one-bit quantization has low power consumption and hardware cost, it significantly limits the SE performance [3], [20]. In this regard, it was shown in [3] that an error floor exists at high SNR for the channel estimator due to coarse quantization and that at least 2–3 times the number of antennas is required to attain an SE comparable to that of a full-resolution system.

The limitations of one-bit quantization have sparked widespread interest and research on low-resolution systems

The authors are with the Centre for Wireless Communications, University of Oulu, Finland (e-mail: {mengyuan.ma, nhan.nguyen, italo.atzeni, markku.juntti}@oulu.fi). This work was supported by the Research Council of Finland (318927 6G Flagship, 332362 EERA, 336449 Profi6, 348396 HIGH-6G, and 357504 EETCAMD).

with multi-bit (2–4 bits) quantization. It was shown in [15], [21] that a system using very few bits can approach the performance of a full-resolution one. Mezghani *et al.* [22] derived a closed-form lower bound for the capacity of a point-to-point MIMO system. More recent works focused on beamforming designs [23]–[25]. Furthermore, mixed-ADC systems, which simultaneously deploy one-bit and high-resolution ADCs, are shown to perform better than fixed-resolution architectures, especially at high SNR [26]–[28]. On the other hand, variable-resolution ADCs have been studied in [12], [14], [29]–[33] to flexibly balance the SE-EE tradeoff of low-resolution systems. For instance, it was shown in [29]–[32] that efficient bit allocation strategies can offer a higher EE compared with uniform-resolution architectures. Castañeda *et al.* [12] developed a resolution-adaptive fully digital receiver within an application-specific integrated circuit (ASIC). Furthermore, they demonstrated that a 256-antenna base station with resolution-adaptive ADCs serving 16 users allows to reduce the power consumption by 6.7 times compared with a traditional fixed-resolution design [14]. Additionally, the gain in SE can be achieved by jointly optimizing the transmit power and ADC resolutions [33].

Many of the aforementioned works utilize the arcsine law [34] to facilitate the analysis and design of one-bit systems. For systems with a few bits, two primary methods are used to model quantization, i.e., the additive quantization noise model (AQNM) [20], [35], [36] and the Bussgang decomposition [37]. Both the two approaches approximate the (nonlinear) quantization function with a linear model. However, in the literature, there are two distinct linear approximations referred to as the AQNM. The first is [35]

$$Q(X) = X + q, \quad (1)$$

where  $Q(\cdot)$  and  $q$  denote the quantization function *quantization error*, respectively. The second is [36]

$$Q(X) = \alpha X + \eta, \quad (2)$$

where  $\alpha$  is a constant depending on the quantizers and on the distribution of  $X$ , and  $\eta$  represents the *quantization distortion* (QD). Both (1) and (2) can be employed to analyze the worst-case system performance [38], [39] assuming that  $q$  or  $\eta$  is a Gaussian variable uncorrelated with  $X$ . Model (2) was first derived in [36] and named AQNM later in [20]; it was also called the pseudo-quantization noise model in [26]. Although (2) and Bussgang decomposition were developed from separate technical lineages, it was shown in [40] that the former is nothing but the latter tailored for the case of quantization. Therefore, we call the model in (2) as the *Bussgang-based AQNM* (BAQNM) while we refer to (1) as the AQNM for distinction. The AQNM is typically less accurate than the BAQNM because the assumption that  $q$  is uncorrelated with  $X$  is generally not satisfied. In contrast,  $\eta$  is uncorrelated with  $X$  based on the properties of the Bussgang decomposition. Furthermore, the QD covariance is a key ingredient for the performance analysis and optimization with the BAQNM. A diagonal approximation of the QD covariance matrix was derived in [22], [29], which has since then been widely used in the literature. However, the error arising from this diagonal

approximation can be substantial in some cases, raising a major concern about the reliability of the corresponding results [33], [40].

## B. Contributions

Previous works [23]–[25], [29], [31], [32] focus on either beamforming design [23]–[25] or bit allocation [29], [31], [32]. The joint optimization of the two aspects is promising to achieve higher SE and provide deeper insights into the SE-EE tradeoff, as shown in [30], [33]. However, the transmitter design was not considered in [30], whereas in [33] the receive beamforming was omitted. Unlike previous studies, this paper focuses on analyzing the BAQNM and the quantization distortion, alongside the joint design of the transmit-receive beamforming and bit allocation for point-to-point MIMO systems utilizing resolution-adaptive ADCs. The specific contributions of this paper are summarized as follows:

- We first identify the essential properties of optimal quantization. Leveraging these properties and the Bussgang decomposition, we reestablish the BAQNM and the diagonal approximation of the QD covariance matrix, offering a new perspective compared to [22], [29]. The analysis shows that the BAQNM and the QD covariance approximation typically hold under the assumption of Gaussian signals undergoing optimal quantization. Furthermore, we examine the connections between applying BAQNM and the arcsine law to one-bit quantization. The consistency in results obtained from these two methods validates our findings.
- Building upon the above theoretical findings, we consider the joint transmit-receive beamforming design and bit allocation problem to maximize the SE subject to the constraints on the transmit power budget and total active bits of ADCs. This design problem is inherently complex due to its mixed-integer nature. We address this by first determining the beamformer under fixed ADC resolutions. Subsequently, we propose a low-complexity algorithm to iteratively optimize the ADC resolutions and the beamforming matrices.
- Extensive numerical simulations verify the superiority of the proposed schemes. Specifically, the results show that the proposed beamforming design significantly outperforms conventional WF solutions in low-resolution systems, especially with one-bit quantization and high SNR. Furthermore, the benefit from bit allocation is clearly demonstrated. For example, in a  $64 \times 64$  MIMO system, the proposed design offers 6% improvement in both SE and EE, while requiring 40% fewer active ADC bits compared with uniform bit allocation. When using a total of 128 bits over the 64 RF chains, the former achieves improvements of 49% in SE and 39% in EE compared to the latter. Moreover, the SE-EE comparison shows that receiving more data streams with low-resolution ADCs can achieve higher SE and EE than receiving fewer data streams with high-resolution ADCs.

### C. Organization and Notations

The rest of this paper is organized as follows. In Section II, we present the signal model and quantization model. The BAQNM and the approximation of the QD covariance are then derived in Section III. We delve into the joint transmit-receive beamforming and bit allocation design in Section IV. Finally, we provide simulation results and conclusions in Sections V and VI, respectively.

Scalars, vectors, and matrices are denoted by the lowercase, boldface lowercase, and boldface uppercase letters, respectively. Furthermore, we use  $(\cdot)^*$ ,  $(\cdot)^T$ ,  $(\cdot)^H$ , and  $(\cdot)^{-1}$  to represent the conjugate, transpose, conjugate transpose, and matrix inverse operators, respectively.  $\|\cdot\|_{\mathcal{F}}$  signify the Frobenius norm for matrices. In addition, the expectation and trace operators are represented by  $\mathbb{E}(\cdot)$  and  $\text{Tr}(\cdot)$ . We use  $|a|$  and  $\det(\mathbf{A})$  to denote the absolute value of the scalar  $a$  and the determinant of matrix  $\mathbf{A}$ , respectively. The real and imaginary part operators are denoted by  $\Re\{\cdot\}$  and  $\Im\{\cdot\}$ , respectively. Moreover,  $\text{diag}(\mathbf{a})$  yields a diagonal matrix with its diagonal entries being the elements of  $\mathbf{a}$ , while  $\text{diag}(\mathbf{A})$  returns a vector with its elements being the diagonal entries of  $\mathbf{A}$ . Finally, we use  $\mathbf{C}_{xy}$  and  $\mathbf{C}_x$  to represent the cross-covariance matrix between  $\mathbf{x}$  and  $\mathbf{y}$  and the auto-covariance matrix of  $\mathbf{x}$ , respectively.

## II. SYSTEM MODEL

### A. System Model

We consider a point-to-point MIMO system where a transmitter (Tx) with  $N_t$  antennas communicates with a receiver (Rx) with  $N_r$  antennas. We assume that the Tx is equipped with high-resolution digital-to-analog converters while low-resolution ADCs are deployed at the Rx. Let  $\mathbf{s} \in \mathbb{C}^{N_s}$  ( $N_s \leq \min(N_t, N_r)$ ) be the transmitted signal vector. We assume that  $\mathbf{s}$  follows the Gaussian distribution and  $\mathbb{E}[\mathbf{s}\mathbf{s}^H] = \mathbf{I}$ . Furthermore, let  $\mathbf{F} \in \mathbb{C}^{N_t \times N_s}$  be the precoding matrix with the power constraint  $\|\mathbf{F}\|_{\mathcal{F}}^2 \leq P_t$ . Here,  $P_t$  denotes the transmit power budget of the Tx. The received signal (without quantization) at the Rx can be written as

$$\mathbf{y} = \mathbf{H}\mathbf{F}\mathbf{s} + \mathbf{n}, \quad (3)$$

where  $\mathbf{H} \in \mathbb{C}^{N_r \times N_t}$  denotes the channel between the Tx and the Rx, and  $\mathbf{n}$  denotes the additive white Gaussian noise (AWGN) vector,  $\mathbf{n} \sim \mathcal{CN}(0, \sigma_n^2 \mathbf{I})$ , with  $\sigma_n^2$  being the noise power. Here, we assume that  $\mathbf{H}$  is quasi-flat during each coherence time. Furthermore, to characterize the system performance bound, we assume the availability of perfect CSI at both the Rx and the Tx [16], [25]. Channel estimation with adaptive-resolution ADCs was studied in [41]. Furthermore, an ASIC receiver integrating both resolution-adaptive ADCs and a channel estimation module was developed in [12].

### B. Signal Model with Quantization

We denote the codebook of a scalar quantizer of  $b$  bits as  $\mathcal{C} = \{c_0, \dots, c_{N_q-1}\}$ , where  $N_q = 2^b$  is the number of output levels of the quantizer. The set of quantization thresholds is  $\mathcal{T} = \{t_0, \dots, t_{N_q}\}$ , where  $t_0 = -\infty$  and  $t_{N_q} = \infty$  allows

inputs with arbitrary power.<sup>1</sup> Let  $Q(\cdot)$  denote the quantization function associated with  $\mathcal{C}$  and  $\mathcal{T}$ . For a complex signal  $x$ , we have  $Q(x) = Q(\Re\{x\}) + jQ(\Im\{x\})$ , with  $Q(\Re\{x\}) = c_{I(\Re\{x\})}$ , where  $I(\Re\{x\}) = i \in \{0, \dots, N_q - 1\}$  for  $\Re\{x\} \in [t_i, t_{i+1}]$ .  $Q(\Im\{x\})$  is obtained in a similar way.

The Bussgang decomposition applied to a vector space in the complex domain is presented in [40]. Specifically, let  $\mathbf{Q} : \mathbb{C}^N \rightarrow \mathbb{C}^N$  denote a scalar quantization function and  $\mathbf{z}$  be the quantized output of  $\mathbf{y}$ . We can write  $\mathbf{z} = \mathbf{Q}(\mathbf{y})$  or equivalently  $z_i = Q_i(y_i)$ ,  $\forall i$ , where  $z_i$  and  $y_i$  denote the  $i$ -th element of  $\mathbf{z}$  and  $\mathbf{y}$ , respectively;  $Q_i(\cdot)$  represents the associated quantization function. For the circular-symmetric Gaussian random vector  $\mathbf{y}$ , the Bussgang decomposition implies

$$\mathbf{z} = \mathbf{Q}(\mathbf{y}) = \mathbf{G}\mathbf{y} + \boldsymbol{\eta}, \quad (4)$$

where  $\mathbf{G} \triangleq \mathbf{C}_{zy}\mathbf{C}_y^{-1}$  denotes the Bussgang gain, and the distortion term  $\boldsymbol{\eta}$  is uncorrelated to  $\mathbf{y}$ . In (4),  $\boldsymbol{\eta}$  represents the QD vector with its covariance matrix given by

$$\mathbf{C}_{\boldsymbol{\eta}} = \mathbb{E}[(\mathbf{z} - \mathbf{G}\mathbf{y})(\mathbf{z} - \mathbf{G}\mathbf{y})^H] = \mathbf{C}_z - \mathbf{G}\mathbf{C}_{yz}. \quad (5)$$

Furthermore, under some mild assumptions, the Bussgang gain  $\mathbf{G}$  is shown to be diagonal, as detailed in the following lemma.

**Lemma 1** ([24], [40], [42]) *Consider a jointly circularly symmetric Gaussian random vector  $\mathbf{y}$  fed into scalar quantizers. With (4) modeling the quantization, we have  $\mathbf{G} = \text{diag}(\mathbf{g})$  with  $g_i = \frac{\mathbb{E}[Q_i(y_i)y_i^*]}{\mathbb{E}[|y_i|^2]}$  being the  $i$ -th element of  $\mathbf{g}$ .*

Substituting (3) into (4), we obtain the quantized version of the signal received at the Rx, expressed as

$$\mathbf{z} = \mathbf{G}\mathbf{H}\mathbf{F}\mathbf{s} + \mathbf{e}, \quad (6)$$

where  $\mathbf{e} = \mathbf{G}\mathbf{n} + \boldsymbol{\eta}$  represents the effective noise with covariance matrix  $\mathbf{C}_e = \mathbb{E}[\mathbf{e}\mathbf{e}^H] = \mathbf{C}_{\boldsymbol{\eta}} + \sigma_n^2 \mathbf{G}^2$ . The post-combined signal at the Rx is expressed as

$$\hat{\mathbf{s}} = \mathbf{U}^H \mathbf{z} = \mathbf{U}^H \mathbf{G}\mathbf{H}\mathbf{F}\mathbf{s} + \mathbf{U}^H \mathbf{e}, \quad (7)$$

where  $\mathbf{U} \in \mathbb{C}^{N_r \times N_t}$  denotes the combining matrix. Although  $\mathbf{s}$  is Gaussian distributed,  $\mathbf{e}$  does not follow a Gaussian distribution because of the non-linear quantization distortion. However, we can treat the effective noise vector  $\mathbf{e}$  as a Gaussian variable and obtain a lower bound of the SE as [39]

$$R = \log \det (\mathbf{I} + (\mathbf{U}^H \mathbf{C}_e \mathbf{U})^{-1} \mathbf{U}^H \mathbf{G}\mathbf{H}\mathbf{F}\mathbf{F}^H \mathbf{H}^H \mathbf{G}\mathbf{U}). \quad (8)$$

It is observed that the Bussgang gain  $\mathbf{G}$  and the QD covariance matrix  $\mathbf{C}_{\boldsymbol{\eta}}$  are necessary for further analysis and optimization of the SE performance. For one-bit quantization, closed-form expressions for  $\mathbf{G}$  and  $\mathbf{C}_{\boldsymbol{\eta}}$  can be derived based on the arcsine law [3]. However, obtaining those for multi-bit quantization is significantly more challenging. A closed-form expression of  $\mathbf{G}$  and a diagonal approximation of  $\mathbf{C}_{\boldsymbol{\eta}}$  were developed in [22], [29] under the assumption that the quantizer

<sup>1</sup>In practice, the input signal of ADCs outside the range  $[t_1, t_{N_q-1}]$  can be clipped into the range of  $[t_1 - \delta, t_{N_q-1} + \delta]$  where  $\delta$  is an adjustable parameter depending on the constraints of hardware components, e.g., the automatic gain control (AGC).

satisfies the following properties:

$$\mathbb{E}[z_i - y_i] = 0, \quad (9)$$

$$\mathbb{E}[(z_i - y_i)z_i] = 0, \quad (10)$$

where  $z_i = Q_i(y_i)$ . However, the validity of these assumptions remains unclear, and thus the applicability of these results to general signal distributions and quantizers is uncertain. In the next section, we derive the BAQNM and diagonal approximation from a new perspective, aiming to clarify this uncertainty.

### III. BAQNM AND APPROXIMATION OF THE QD COVARIANCE

In this section, we first identify the fundamental properties of optimal quantizers in Lemma 2 and Lemma 3 and then leverage them to obtain the BAQNM and the approximation of the QD covariance. Furthermore, we elaborate on the nuances between applying the BAQNM and the arcsine law to one-bit quantization.

#### A. Properties of Optimal Quantizers

We first recall the definition of the optimal quantizer [43] below.

**Definition 1 ([43])** Consider a real-valued random variable  $X$ . Let  $f_X(x)$  denote its probability density function (PDF), and let  $Q(x) = c_{I(x)}$  be its quantized approximation, where  $I(x) = i \in \{0, \dots, N_q - 1\}$  satisfies  $x \in (t_i, t_{i+1}]$ . The mean square error (MSE) for the quantization can be expressed as

$$D = \mathbb{E}[(Q(x) - x)^2] = \sum_{i=0}^{N_q-1} \int_{t_i}^{t_{i+1}} (x - c_i)^2 f_X(x) dx. \quad (11)$$

The optimal quantizer is the one that minimizes  $D$ .

By setting the derivatives of  $D$  with respect to  $t_j$  and  $c_j$  to zeros, we obtain

$$t_j = \frac{c_j + c_{j-1}}{2}, \quad (12)$$

$$c_j = \frac{\int_{t_j}^{t_{j+1}} x f_X(x) dx}{\int_{t_j}^{t_{j+1}} f_X(x) dx}, \quad (13)$$

which are referred to as the *nearest neighbor condition* and the *centroid condition*, respectively, [35, Chapter 6]. They are necessary for the optimal quantizer, also known as the Lloyd-Max quantizer [43] or the optimal non-uniform quantizer. The latter term follows the fact that the optimal quantizer is generally non-uniform. The uniform quantizer that minimizes  $D$  in (11) is referred to as the optimal uniform quantizer.

**Remark 1** The centroid condition requires that the output of the quantization for each interval is its mean value. This condition can also be written as [35]

$$\mathbb{E}[X|Q(X)] = Q(X), \quad (14)$$

which was used in [36] as a basic assumption for deriving the model (2). Therefore, the BAQNM is limited to the optimal quantizer.

The Lloyd-Max algorithm [43] iteratively updates  $\mathcal{T}$  and  $\mathcal{C}$  based on (12) and (13) to find the optimal quantizer for a specific input signal. However, this iterative method requires a long run time, especially for high-resolution quantization. In what follows, we propose an optimal quantization without running the Lloyd-Max algorithm. To this end, we begin with identifying the fundamental properties for the optimal quantization of Gaussian signals in the following lemma.

**Lemma 2** Let  $X$  be a real-valued, zero-mean, and unit-variance random variable, and let  $Y = \sigma_y X$ . Then, we have

$$Q_y(Y) = \sigma_y Q_x(X) = \sigma_y Q_x\left(\frac{Y}{\sigma_y}\right), \quad (15)$$

$$\gamma = \mathbb{E}[(Q_x(X) - X)^2] = \frac{\mathbb{E}[(Q_y(Y) - Y)^2]}{\sigma_y^2}, \quad (16)$$

where  $Q_y(Y)$  and  $Q_x(X)$  denote the optimal quantized output of  $Y$  and  $X$ , respectively.

*Proof:* See Appendix A. ■

We refer to  $\gamma$  as the *distortion factor* and the properties in (15) and (16) as the *scaling property* and *distortion invariance*, respectively. Utilizing the scaling property and the optimal quantizer for the standard Gaussian signal [43], we can derive the optimal quantization for any Gaussian signal with a known variance. For example, we can obtain the optimal element-wise quantization of the received signal vector  $\mathbf{y}$  in (3) with covariance matrix

$$\mathbf{C}_y \triangleq \mathbb{E}[\mathbf{y}\mathbf{y}^H] = \mathbf{H}\mathbf{F}\mathbf{F}^H\mathbf{H}^H + \sigma_n^2\mathbf{I}. \quad (17)$$

Regarding the distortion factor, we note the following property.

**Lemma 3** For a zero-mean complex random variable  $X = \Re\{X\} + j\Im\{X\}$  with variance  $\sigma_X^2$ , assume that  $\Re\{X\}$  and  $\Im\{X\}$  are independent and identically distributed (i.i.d.) with the same variance  $\frac{\sigma_X^2}{2}$  and are independently quantized by two identical Lloyd-Max quantizers  $Q(\cdot)$ . With  $\chi \triangleq Q(X) - X$ , we obtain

$$\mathbb{E}[Q(X)] = \mathbb{E}[X], \quad (18)$$

$$\mathbb{E}[Q(X)\chi^*] = 0, \quad (19)$$

$$\gamma = \frac{\mathbb{E}[|\chi|^2]}{\mathbb{E}[|X|^2]} = \frac{\mathbb{E}[\Re\{\chi\}^2]}{\mathbb{E}[\Re\{X\}^2]} = \frac{\mathbb{E}[\Im\{\chi\}^2]}{\mathbb{E}[\Im\{X\}^2]}. \quad (20)$$

*Proof:* See Appendix B. ■

Lemma 2 and Lemma 3 reveal the fundamental properties of the optimal quantization of Gaussian signals that have not been previously introduced in the literature. Lemma 2 also holds for the optimal uniform quantizer. The same cannot be concluded for Lemma 3 because it is derived based on the centroid condition (13). However, we will later numerically verify that Lemma 3 still approximately holds for the optimal uniform quantizer. Next, we derive the BAQNM and the approximation of the QD covariance.

#### B. BAQNM and Approximation of the QD Covariance

Some of the results derived in this section will be used in Section IV for the joint beamforming design and bit allocation.

Building on Lemmas 1 and 3, we can obtain a closed-form expression for the Bussgang gain matrix  $\mathbf{G}$ , as in the following lemma.

**Lemma 4** For a zero-mean Gaussian signal vector  $\mathbf{y} = [y_1, \dots, y_N]^T \in \mathbb{C}^N$ , assume that the real and imaginary parts of  $y_i$  have the same variance and are independently quantized by two identical Lloyd-Max quantizers  $Q_i(\cdot)$ . Define  $\mathbf{q} = [q_1, \dots, q_N]^T$  with  $q_i = Q_i(y_i) - y_i, \forall i$  being the quantization error. The Bussgang gain matrix  $\mathbf{G}$  is given by

$$\mathbf{G} = \mathbf{I} - \mathbf{\Gamma}, \quad (21)$$

where  $\mathbf{\Gamma} = \text{diag}(\gamma_1, \dots, \gamma_N)$  with  $\gamma_i = \frac{\mathbb{E}[|q_i|^2]}{\mathbb{E}[|y_i|^2]}$  being the distortion factor of the  $i$ -th pair of quantizers.

*Proof:* With Lemma 1, we have  $\mathbf{G} = \text{diag}(g_1, \dots, g_N)$  and  $g_i = \frac{\mathbb{E}[Q_i(y_i)y_i^*]}{\mathbb{E}[|y_i|^2]}, \forall i$ . Therefore, we have

$$\begin{aligned} g_i &= \frac{\mathbb{E}[Q_i(y_i)y_i^*]}{\mathbb{E}[|y_i|^2]} = \frac{\mathbb{E}[(y_i + q_i)y_i^*]}{\mathbb{E}[|y_i|^2]} \\ &\stackrel{(d)}{=} 1 + \frac{\mathbb{E}[q_i(y_i - Q_i(y_i))^*]}{\mathbb{E}[|y_i|^2]} = 1 - \frac{\mathbb{E}[|q_i|^2]}{\mathbb{E}[|y_i|^2]} = 1 - \gamma_i, \end{aligned} \quad (22)$$

where (d) follows from (19). ■

Lemma 4 indicates that for Gaussian signals under the optimal quantization, the Bussgang gain depends only on the resolutions of the quantizers. Once the quantizer resolutions across the RF chains are determined, we can easily obtain  $\mathbf{G}$ . The value of the distortion factor for  $b \in \{1, \dots, 5\}$  can be found in [43]. For the optimal quantizer with more than 5 bits, it was shown that its distortion factor can be approximated as [35, Chapter 6]

$$\gamma(b) \approx \frac{\sqrt{3}\pi}{2} 2^{-2b}, \quad (23)$$

where we omit the subscript  $i$  without loss of generality and explicitly express  $\gamma$  as a function of  $b$  for clarity. Unlike the high-resolution approximation of the distortion factor in (23), we herein present an approximation that is also valid for low-resolution cases. Specifically, the distortion factors of both the Lloyd-Max and the optimal uniform quantizer can be approximated as

$$\gamma(b) \approx 2^{-1.74b+0.28}. \quad (24)$$

Fig. 1(a) shows the approximated distortion factors by (23) and (24) compared with the accurate ones of the Lloyd-Max quantizer and the optimal uniform quantizer. It can be observed that the distortion factors of the Lloyd-Max quantizer and optimal uniform quantizer are comparable. The proposed approximation (24) can well approach the accurate value of the distortion factors while the approximation (23) becomes increasingly inaccurate for fewer bits. For more than five bits, both approximations closely match the theoretical value of the distortion factor, which is omitted from the figure.

With Lemma 4, (4) can be recast as

$$\mathbf{z} = (\mathbf{I} - \mathbf{\Gamma})\mathbf{y} + \boldsymbol{\eta}, \quad (25)$$

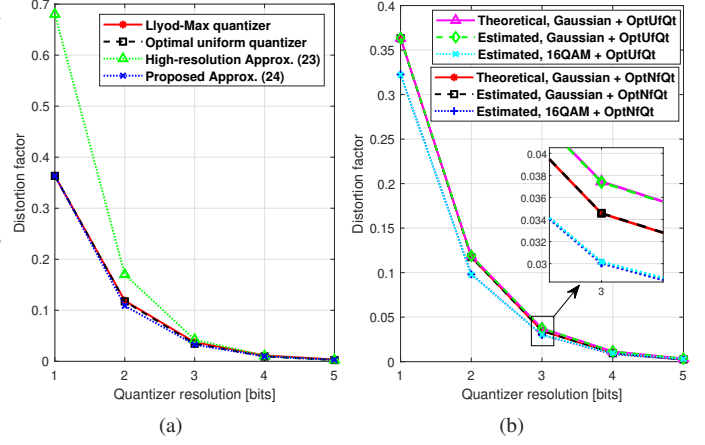


Fig. 1. Distortion factor versus the quantizer resolution  $b$ . Fig. (a) shows the accuracy of the approximated distortion factor. Fig. (b) shows the accuracy of the estimated distortion factor in an example with  $N_r = N_t = 16$  and  $N_s = 4$ .

which is exactly the vector form of the BAQNM. Furthermore, with (25), we obtain

$$\boldsymbol{\eta} = \mathbf{z} - (\mathbf{I} - \mathbf{\Gamma})\mathbf{y} = \mathbf{q} + \mathbf{\Gamma}\mathbf{y}, \quad (26)$$

which yields

$$\mathbf{C}_\eta = \mathbb{E}[(\mathbf{q} + \mathbf{\Gamma}\mathbf{y})(\mathbf{q} + \mathbf{\Gamma}\mathbf{y})^H] = \mathbf{C}_q - \mathbf{\Gamma}\mathbf{C}_y\mathbf{\Gamma}, \quad (27)$$

$$\mathbf{C}_z = \mathbf{C}_q + (\mathbf{I} - \mathbf{\Gamma})\mathbf{C}_y - \mathbf{C}_y\mathbf{\Gamma}, \quad (28)$$

where  $\mathbf{C}_q$  and  $\mathbf{C}_z$  denotes the covariance matrix of  $\mathbf{q}$  and  $\mathbf{z}$ , respectively. As the covariance matrix  $\mathbf{C}_y$  can usually be estimated as a prior, we can obtain closed-form expressions for  $\mathbf{C}_\eta$  and  $\mathbf{C}_z$  by approximating  $\mathbf{C}_q$ . The details are presented below.

**Lemma 5** For a circular-symmetric Gaussian vector  $\mathbf{y}$ , assume that the Lloyd-Max quantizers are adopted for each element of  $\mathbf{y}$ . The following approximations hold:

$$\mathbf{C}_q \approx \mathbf{\Gamma}\mathbf{C}_y\mathbf{\Gamma} + (\mathbf{I} - \mathbf{\Gamma})\text{diag}(\mathbf{C}_y)\mathbf{\Gamma}, \quad (29)$$

$$\mathbf{C}_\eta \approx \mathbf{\Gamma}\text{diag}(\mathbf{C}_y)(\mathbf{I} - \mathbf{\Gamma}), \quad (30)$$

$$\mathbf{C}_z \approx [\text{diag}(\mathbf{C}_y)\mathbf{\Gamma} + (\mathbf{I} - \mathbf{\Gamma})\mathbf{C}_y](\mathbf{I} - \mathbf{\Gamma}). \quad (31)$$

The diagonal entries of  $\mathbf{C}_\eta$  are accurate. The approximation of  $\mathbf{C}_\eta$  is due to neglecting its non-zero off-diagonal entries.

*Proof:* See Appendix C. ■

We note that the BAQNM and the QD covariance approximation in (25) and Lemma 5 coincide with those in [22], [29]. However, unlike these existing works, we reestablish the BAQNM and closed-form approximations of  $\mathbf{C}_q$ ,  $\mathbf{C}_\eta$ , and  $\mathbf{C}_z$  from the properties of the optimal quantization of Gaussian signals, offering new perspectives on the derivations. The analysis unveils that the BAQNM and the diagonal approximation of the QD covariance matrix typically hold for a circularly symmetric Gaussian random vector quantized by the Lloyd-Max quantizers.<sup>2</sup> Building on this condition, we will perform the joint beamforming design and bit allocation based on (21)

<sup>2</sup>We note that the BAQNM and the diagonal approximation of the QD covariance matrix approximately hold for Gaussian signals under the optimal uniform quantizers. This is because Lemma 3 approximately holds for the optimal uniform quantizer, as verified in Fig. 1(b).

and (30) in Section IV. Furthermore, it is worth noting that without the condition, the system performance characterized based on the BAQNM and the diagonal approximation of  $\mathbf{C}_\eta$  becomes less reliable.

As an example, Fig. 1(b) shows the simulated distortion factors for Gaussian signaling and signaling of 16-quadrature amplitude modulation (16QAM) in comparison with the theoretical value. Both types of received signals are quantized by the optimal non-uniform quantizer (OptNfQt) and the optimal uniform quantizer (OptUfQt) [43] at the Rx. The simulated distortion factor is obtained as  $\frac{1}{7} \sum_{i=1}^I \frac{|s^{(i)} - s_q^{(i)}|^2}{|s^{(i)}|^2}$  where  $s^{(i)}$  and  $s_q^{(i)}$  denote the  $i$ -th received signal sample and the quantized one, with  $I = 10^5$ . It is seen that the estimated distortion factors for Gaussian signaling align well with the theoretical values, while those for 16QAM signaling yield smaller values due to the mismatch between the signal distribution and the quantizers. Such a mismatch also renders the diagonal approximation of the QD covariance matrix less accurate.

### C. One-Bit Case

The above discussion and the results in Lemma 5 also valid for the one-bit quantization. Thereby, the closed-form expressions of  $\mathbf{G}$  and  $\mathbf{C}_\eta$  and their connection to the arcsine law can be shown. We first recall the widely used results for one-bit quantization in the next lemma.

**Lemma 6** ([3], [19], [44]) *Denote the one-bit quantization function as  $Q(\mathbf{y}) = \sqrt{\frac{\beta}{2}} [\text{sgn}(\Re\{\mathbf{y}\}) + j\text{sgn}(\Im\{\mathbf{y}\})]$ , where  $\text{sgn}(\cdot)$  returns the signs of the real and imaginary parts of each element of  $\mathbf{y}$ . Let  $\mathbf{z} \triangleq Q(\mathbf{y})$ . The following equality hold:*

$$\mathbf{C}_{zy} = \sqrt{\frac{2\beta}{\pi}} \mathbf{K}^{-\frac{1}{2}} \mathbf{C}_y, \quad (32)$$

$$\mathbf{C}_z = \frac{2\beta}{\pi} \arcsin(\mathbf{K}^{-\frac{1}{2}} \mathbf{C}_y \mathbf{K}^{-\frac{1}{2}}), \quad (33)$$

$$\text{diag}(\mathbf{C}_z) = \beta \mathbf{I}, \quad (34)$$

where  $\mathbf{K} = \text{diag}(\mathbf{C}_y)$ , and the arcsine function is element-wise applied to its matrix argument.

Writing  $\mathbf{z} = \mathbf{G}\mathbf{y} + \boldsymbol{\eta}$ , we can obtain

$$\mathbf{G} = \sqrt{\frac{2\beta}{\pi}} \mathbf{K}^{-\frac{1}{2}}, \quad (35)$$

$$\mathbf{C}_\eta = \frac{2\beta}{\pi} \arcsin(\mathbf{K}^{-\frac{1}{2}} \mathbf{C}_y \mathbf{K}^{-\frac{1}{2}}) - \frac{2\beta}{\pi} \mathbf{K}^{-\frac{1}{2}} \mathbf{C}_y \mathbf{K}^{-\frac{1}{2}}. \quad (36)$$

We note that the quantization in Lemma 6 is generally not optimal because all the elements of the signal vector  $\mathbf{y}$ , even with different variances, yield the same output levels after quantization. In contrast, the quantization in Lemma 5 indicates that elements of  $\mathbf{y}$  are optimally quantized, generating output levels according to their variances. However, the results of Lemmas 5 and 6 coincide in some circumstances. For example, define a general one-bit quantizer as

$$Q(x) = \begin{cases} c & \text{if } x \geq 0, \\ -c & \text{if } x < 0. \end{cases} \quad (37)$$

For a complex random vector  $\mathbf{y} \sim \mathcal{CN}(\mathbf{0}, \sigma_Y^2 \mathbf{I})$ , we can obtain the optimal one-bit quantizer as  $c = \sqrt{\frac{2}{\pi}} \sigma_Y$  based on conditions (12) and (13). According to (15), the optimal one-bit quantized output can be written as

$$Q(\mathbf{y}) = \frac{\sigma_Y}{\sqrt{\pi}} \left( \text{sgn} \left( \frac{\sqrt{2}}{\sigma_Y} \Re\{\mathbf{y}\} \right) + j \text{sgn} \left( \frac{\sqrt{2}}{\sigma_Y} \Im\{\mathbf{y}\} \right) \right). \quad (38)$$

Because  $\mathbf{C}_y = \sigma_Y^2 \mathbf{I}$  has identical diagonal entries,  $\mathbf{C}_\eta$  is also a diagonal matrix [42]. Therefore, Lemma 5 yields accurate  $\mathbf{C}_\eta$ . Based on (21) and (30), we have

$$\mathbf{G} = 0.6366 \mathbf{I}, \quad \mathbf{C}_\eta = 0.2313 \sigma_Y^2 \mathbf{I}. \quad (39)$$

Furthermore, by setting  $\sqrt{\frac{\beta}{2}} = \sqrt{\frac{2}{\pi}} \sigma_Y$ , i.e.,  $\beta = \frac{2}{\pi} \sigma_Y^2$ , we can obtain the optimal quantization in Lemma 6. Based on (35) and (36), the resulting  $\mathbf{G}$  and  $\mathbf{C}_\eta$  are the same as those in (39). This alignment justifies our findings in Section III-B.

## IV. JOINT BEAMFORMING DESIGN AND BIT ALLOCATION

We showed in Section III that the BAQNM and the closed-form approximation of the QD covariance matrix hold under the assumption of Gaussian signals undergoing optimal quantization. With this assumption, we obtain the closed-form expression of the SE based on (21) and (30), which enable us to proceed with the joint design of transmit-receive beamforming and bit allocation in this section. The design problem is formulated next.

### A. Problem Formulation

Building on Lemma 5, the covariance matrix of the QD vector in (5) can be approximated as

$$\mathbf{C}_\eta \approx \mathbf{G} (\mathbf{I} - \mathbf{G}) \text{diag}(\mathbf{C}_y), \quad (40)$$

leading to the following approximation of the covariance matrix of the effective noise vector:

$$\mathbf{C}_e \approx \mathbf{G} (\mathbf{I} - \mathbf{G}) \text{diag}(\mathbf{H}\mathbf{F}\mathbf{F}^H\mathbf{H}^H) + \sigma_n^2 \mathbf{G}. \quad (41)$$

This approximation becomes more accurate with higher-resolution ADCs. Define  $\mathbf{b} \triangleq [b_1, \dots, b_{N_r}]$  with  $b_i$  being the resolution of the  $i$ -th pair of ADCs. Let  $\mathcal{B} \triangleq \{1, \dots, b_{\max}\}$  be the set of possible ADC resolutions allocated to an RF chain. Moreover, let  $b_{\text{total}}$  be the total number of ADC bits available for all RF chains. The joint design of transmit-receive beamformers and bit allocation is formulated as:

$$\underset{\mathbf{b}, \mathbf{F}, \mathbf{U}}{\text{maximize}} \quad R \quad (42a)$$

$$\text{subject to} \quad \|\mathbf{F}\|_{\mathcal{F}}^2 \leq P_t, \quad (42b)$$

$$\sum_{i=1}^{N_r} b_i = \lfloor \varsigma b_{\text{total}} \rfloor, \quad (42c)$$

$$b_i \in \mathcal{B}, \quad i = 1, \dots, N_r, \quad (42d)$$

where  $R$  is given in (8), and  $\varsigma \in (0, 1]$  is the fraction of active bits so that the total number of active bits is  $\lfloor \varsigma b_{\text{total}} \rfloor$ . Here,  $\lfloor x \rfloor$  denotes the nearest integer smaller than  $x$ . Problem (42) has a mixed-integer nature and coupled variables in the objective function, making it challenging to solve. Observing that the design of  $\{\mathbf{F}, \mathbf{U}\}$  depends on  $\mathbf{b}$ , we propose a two-stage optimization framework wherein we first solve  $\{\mathbf{F}, \mathbf{U}\}$

with a given  $\mathbf{b}$ , and then find an efficient solution to  $\mathbf{b}$  based on the proposed beamforming algorithm. The details are elaborated next.

### B. Proposed Solution for (42)

1) *Beamforming Design:* For a given  $\mathbf{b}$ , the Busgang gain matrix  $\mathbf{G}$  is fixed according to Lemma 4. Therefore, the beamformers  $\{\mathbf{F}, \mathbf{U}\}$  can be obtained by solving the following problem:

$$\underset{\mathbf{F}, \mathbf{U}}{\text{maximize}} R, \text{ subject to (42b),} \quad (43)$$

which is non-convex. To address it, we transform the objective function into a more tractable form with the following proposition.

**Proposition 1** *The MSE matrix of the post-combined signals at the Rx is given by*

$$\mathbf{E} \triangleq \mathbb{E}[(\hat{\mathbf{s}} - \mathbf{s})(\hat{\mathbf{s}} - \mathbf{s})^H] = \mathbf{U}^H (\mathbf{G}\mathbf{H}\mathbf{F}\mathbf{F}^H\mathbf{H}^H\mathbf{G} + \mathbf{C}_e) \mathbf{U} + \mathbf{I} - \mathbf{U}^H\mathbf{G}\mathbf{H}\mathbf{F} - \mathbf{F}^H\mathbf{H}^H\mathbf{G}\mathbf{U}, \quad (44)$$

where  $\mathbf{C}_e$  is given in (41). Consider the weighted MSE minimization problem

$$\underset{\mathbf{U}, \mathbf{F}, \mathbf{W}}{\text{minimize}} f(\mathbf{U}, \mathbf{F}, \mathbf{W}) \triangleq \text{Tr}(\mathbf{W}\mathbf{E}) - \log \det(\mathbf{W}) \quad (45)$$

subject to (42b),

where  $\mathbf{W} \succeq 0$  is an introduced weighted matrix. The optimal solutions to  $\mathbf{W}$  and  $\mathbf{U}$  are given by

$$\mathbf{W} = \mathbf{I} + \mathbf{F}^H\mathbf{H}^H\mathbf{G}\mathbf{C}_e^{-1}\mathbf{G}\mathbf{H}\mathbf{F}, \quad (46)$$

$$\mathbf{U} = (\mathbf{G}\mathbf{H}\mathbf{F}\mathbf{F}^H\mathbf{H}^H\mathbf{G} + \mathbf{C}_e)^{-1}\mathbf{G}\mathbf{H}\mathbf{F}. \quad (47)$$

It can be shown that the optimal solution for (45) is the same as that for (43).

*Proof:* See Appendix D. ■

Note that  $f(\mathbf{U}, \mathbf{F}, \mathbf{W})$  is convex with respect to one variable when the others are fixed. We use an alternating optimization procedure to solve problem (45). Since the solutions to  $\mathbf{U}$  and  $\mathbf{W}$  are given, we delineate the solution to  $\mathbf{F}$  next. With some algebra, the subproblem of the precoder design can be expressed as

$$\underset{\mathbf{F}}{\text{minimize}} \text{Tr}(\mathbf{J}\mathbf{F}\mathbf{F}^H) - 2\Re\{\text{Tr}(\mathbf{W}\mathbf{U}^H\mathbf{G}\mathbf{H}\mathbf{F})\} \quad (48a)$$

$$\text{subject to } \text{Tr}(\mathbf{F}\mathbf{F}^H) \leq P_t, \quad (48b)$$

where  $\mathbf{J} \triangleq \mathbf{H}^H (\mathbf{G}\mathbf{U}\mathbf{W}\mathbf{U}^H + \text{diag}(\mathbf{U}\mathbf{W}\mathbf{U}^H) (\mathbf{I} - \mathbf{G})) \mathbf{G}\mathbf{H}$ . Problem (48) is convex and admits a closed-form solution. Specifically, we first obtain the Lagrangian function as

$$L(\mathbf{F}, \mu) = \text{Tr}(\mathbf{J}\mathbf{F}\mathbf{F}^H) - 2\Re\{\text{Tr}(\mathbf{W}\mathbf{U}^H\mathbf{G}\mathbf{H}\mathbf{F})\} + \mu(\text{Tr}(\mathbf{F}\mathbf{F}^H) - P_t), \quad (49)$$

where  $\mu \geq 0$  is the Lagrangian multiplier. Leveraging the first-order condition of optimality, we obtain

$$\mathbf{F} = (\mathbf{J} + \mu\mathbf{I})^{-1}\mathbf{H}^H\mathbf{G}\mathbf{U}\mathbf{W}, \quad (50)$$

where  $\mu$  satisfying  $\mu(\|\mathbf{F}\|_{\mathcal{F}}^2 - P_t) = 0$  can be obtained via the bisection search on the range  $\left[0, \frac{\|\mathbf{H}^H\mathbf{G}\mathbf{U}\mathbf{W}\|_{\mathcal{F}}}{\sqrt{P_t}}\right]$ .

The alternating optimization procedure for updating  $\mathbf{F}$  and  $\mathbf{U}$ , referred to as AltMin beamforming (AltMin-BF) design, is

---

### Algorithm 1: AltMin Beamforming Design

---

**Output:**  $\mathbf{F}, \mathbf{U}$   
1 Initialize  $\mathbf{b}, \mathbf{F}, \mathbf{W}, \varepsilon$ .  
2 **repeat**  
3      $\mathbf{W}' \leftarrow \mathbf{W}$ .  
4      $\mathbf{U} \leftarrow (\mathbf{G}\mathbf{H}\mathbf{F}\mathbf{F}^H\mathbf{H}^H\mathbf{G} + \mathbf{C}_e)^{-1}\mathbf{G}\mathbf{H}\mathbf{F}$ .  
5      $\mathbf{W} \leftarrow \mathbf{I} + \mathbf{F}^H\mathbf{H}^H\mathbf{G}\mathbf{C}_e^{-1}\mathbf{G}\mathbf{H}\mathbf{F}$ .  
6     Update  $\mathbf{F}$  by (50).  
7 **until**  $|\log \det(\mathbf{W}') - \log \det(\mathbf{W})| \leq \varepsilon$ ;

---

summarized in Algorithm 1. Because the alternating updates of  $\mathbf{W}$ ,  $\mathbf{U}$ , and  $\mathbf{F}$  result in a nondecreasing sequence of objective values, which are upper bounded due to the power constraint, the convergence of Algorithm 1 is guaranteed. We initialize  $\mathbf{F}$  based on the WF method and set  $\mathbf{W} = \mathbf{I}$ .

2) *Bit Allocation:* With  $\mathbf{F}$  and  $\mathbf{U}$  obtained by Algorithm 1, the bit allocation problem is formulated as

$$\underset{\mathbf{b}}{\text{maximize}} R(\mathbf{b}) \quad (51)$$

subject to (42c) and (42d),

where  $R(\mathbf{b})$  represents the SE achieved with  $\mathbf{b}$ . The non-convex integer nature makes problem (51) again challenging to solve. An exhaustive search (ES) can be performed to find the optimal resolutions. However, it requires excessively high complexity.

To overcome the challenge, we propose in Algorithm 2 a low-complexity greedy pair-order search-based beamforming and bit allocation (GPOS-BFBA). Specifically, for initialization, we first assume that all the ADCs employ  $b_{\max}$  bits, i.e.,  $b_i = b_{\max}, \forall i$ . In steps 2–9, the ADC bits in each RF chain are gradually decreased to one until the total bit requirement is reached. This is based on the fact that more resolution bits offer higher SE.

In steps 11–16, a neighbor search procedure is performed to find better solutions for  $\mathbf{b}$  by adjusting the order of every pair of elements (if their values are different) in the bit allocation vector. Specifically, let  $\mathbf{b}^{(\ell)}$  be the candidate in the  $\ell$ -th iteration. We define the set of neighbor points of  $\mathbf{b}^{(\ell)}$  as  $\mathcal{N}(\mathbf{b}^{(\ell)}) \triangleq \left\{ \tilde{\mathbf{b}}^{(\ell)} : \tilde{\mathbf{b}}^{(\ell)} = \mathbf{b}_{[i \leftrightarrow j]}^{(\ell)} \text{ if } b_i^{(\ell)} \neq b_j^{(\ell)}, \tilde{\mathbf{b}}^{(\ell)} \notin \mathcal{L} \right\}$ , (52)

where  $\mathbf{b}_{[i \leftrightarrow j]}^{(\ell)}$  is obtained by swapping the  $i$ -th and  $j$ -th elements of  $\mathbf{b}^{(\ell)}$ , i.e.,

$$\mathbf{b}_{[i \leftrightarrow j]}^{(\ell)} = [b_1^{(\ell)}, \dots, b_{i-1}^{(\ell)}, b_j^{(\ell)}, b_i^{(\ell)}, b_{i+1}^{(\ell)}, \dots, b_{j-1}^{(\ell)}, b_i^{(\ell)}, b_{j+1}^{(\ell)}, \dots, b_{N_r}^{(\ell)}]^\top. \quad (53)$$

Furthermore,  $\mathcal{L} = \cup_{m=1}^{\ell-1} \mathcal{N}(\mathbf{b}^{(m)})$  is the list of the candidates examined in the previous iterations. A neighbor point should not belong to this list to avoid a cycling search. Accordingly, there are at most  $\frac{1}{2}N_r(N_r - 1)$  neighbors in the neighbor set  $\mathcal{N}(\mathbf{b}^{(\ell)})$ . For each neighbor point, the beamformers, i.e.,  $\mathbf{F}$  and  $\mathbf{U}$ , are obtained using Algorithm 1, and the corresponding SE is computed, as in step 13. Then, the best neighbor point  $\mathbf{b}^{(\ell)*}$  that offers the highest SE is found as in step 14. In step 15, the best solution  $\mathbf{b}^*$  can be updated as  $\mathbf{b}^{(\ell)*}$  if the latter achieves a higher SE. This iterative process is repeated for  $\mathcal{L}_2$  iterations or until convergence. Finally, the beamformers and resolutions are returned in step 18.

---

**Algorithm 2:** Greedy pair-order search based beamforming and bit allocation
 

---

**Output:**  $\mathbf{b}^*$ ,  $\mathbf{F}^*$ ,  $\mathbf{U}^*$

- 1 Initialize  $\varsigma$ ,  $b_{\text{total}}$ ,  $b_{\text{max}}$ , and set  $b_i = b_{\text{max}}$ ,  $\forall i$ .
- 2 **for**  $n = 1, \dots, N_r$  **do**
- 3     **while**  $b_n \geq 2$  and  $\sum_{i=1}^{N_r} b_i > \lfloor \varsigma b_{\text{total}} \rfloor$  **do**
- 4          $b_n = b_n - 1$ .
- 5     **end**
- 6     **if**  $\sum_{i=1}^{N_r} b_i = \lfloor \varsigma b_{\text{total}} \rfloor$  **then**
- 7         **break**.
- 8     **end**
- 9 **end**
- 10 Set  $\mathbf{b}^* = [b_1, \dots, b_{N_r}]^T$ ,  $\ell = 1$ ,  $\mathbf{b}^{(\ell)} = \mathbf{b}^*$ .
- 11 **for**  $\ell = 1, \dots, \mathcal{I}_2$  **do**
- 12     Construct the neighbor set  $\mathcal{N}(\mathbf{b}^{(\ell)})$  based on (52).
- 13     Obtain  $\mathbf{F}$  and  $\mathbf{U}$  using Algorithm 1 and the resultant SE for each neighbor point in  $\mathcal{N}(\mathbf{b}^{(\ell)})$ .
- 14     Set  $\mathbf{b}^{(\ell)*}$  to the neighbor point that offers the largest SE.
- 15     Update  $\mathbf{b}^* = \mathbf{b}^{(\ell)*}$  if  $R(\mathbf{b}^{(\ell)*}) > R(\mathbf{b}^*)$ .
- 16     Set  $\mathbf{b}^{(\ell+1)} = \mathbf{b}^*$  as the candidate for the next iteration.
- 17 **end**
- 18 Output  $\{\mathbf{F}^*, \mathbf{U}^*\}$  associated with  $\mathbf{b}^*$ .

---

Through numerical simulations, we found that only a few iterations are sufficient for Algorithm 1 to obtain the best neighbor point in step 14. In such a case, the complexity of the search procedure in steps 11–17 of Algorithm 2 can be greatly reduced. However, Algorithm 1 with a sufficiently large number of iterations is required for the final beamformers. The iterative procedure in Algorithm 1 jointly solves the resolution vector  $\mathbf{b}$  and beamformer  $\{\mathbf{F}, \mathbf{U}\}$  in each iteration to improve system SE, which guarantees nondecreasing SE over iterations.

### C. Complexity Analysis

In massive MIMO systems, we have  $N_s \ll \min(N_t, N_r)$  in general. Thus, the per-iteration complexity of Algorithm 1 can be shown as  $\mathcal{O}(3N_t^3 + 3N_r^3 + 8N_t^2N_r + 8N_tN_r^2)$ , which is mainly due to the computation of matrix multiplication, inverse, and determinants. Therefore, the overall complexity of Algorithm 1 is approximately  $\mathcal{I}_1\mathcal{O}(3N_t^3 + 3N_r^3 + 8N_t^2N_r + 8N_tN_r^2)$ , where  $\mathcal{I}_1$  denotes the total number of iterations required. Since the size of  $\mathcal{N}(\mathbf{b}^{(\ell)})$  is less than  $N_r/2$ , the complexity of Algorithm 2 is approximately  $\mathcal{I}_2\mathcal{I}_1\mathcal{O}(\frac{3}{2}N_t^3N_r^2 + \frac{3}{2}N_r^2 + 4N_t^2N_r^3 + 4N_tN_r^4)$ . Here,  $\mathcal{I}_2$  is the total number of iterations in the search procedure of Algorithm 2. In contrast, the complexity of the ES method for solving problem (51) is  $b_{\text{max}}^{N_r}\mathcal{O}(2N_t^3 + 2N_tN_r^2 + 2N_t^2N_r)$ . Compared to ES, Algorithm 2 has a significant reduction in complexity.

## V. NUMERICAL RESULTS AND DISCUSSION

We herein provide numerical results to demonstrate the performance of the proposed joint beamforming design and bit allocation. We set the carrier frequency and bandwidth to 28 GHz and 1 GHz, respectively. We adopt the Saleh-Valenzuela channel model to characterize the mmWave channel [45], [46]. The channel parameters are set the same as those in [46]. Furthermore, the SNR is defined as  $\text{SNR} \triangleq \frac{P}{\sigma_n^2}$ .

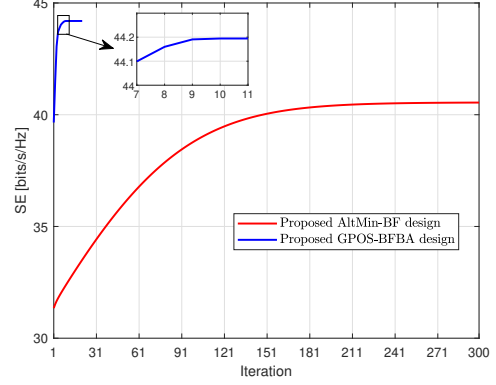


Fig. 2. Convergence of the proposed algorithms with  $N_t = N_r = 64$ ,  $N_s = 8$ , SNR = 10 dB,  $b = 2$ ,  $b_{\text{max}} = 8$ , and  $\varsigma = 1$ .

The other parameters are detailed in each figure. All reported results are averaged over  $10^3$  channel realizations.

For performance comparison, we consider the eigen-mode beamforming scheme with WF power allocation. In this scheme, we set  $\mathbf{U} = \mathbf{Z}(:, 1 : N_s)$  and  $\mathbf{F} = \mathbf{V}(:, 1 : N_s)\mathbf{P}^{\frac{1}{2}}$  where  $\mathbf{Z}$  and  $\mathbf{V}$  are obtained from the singular value decomposition of the channel matrix, i.e.,  $\mathbf{H} = \mathbf{Z}\mathbf{\Sigma}\mathbf{V}^H$ . Furthermore,  $\mathbf{P} \triangleq \text{diag}(p_1, \dots, p_{N_s})$  with  $p_i$  representing the power allocated to the  $i$ -th data stream, obtained by the WF method. In all simulations, we set the same  $b$ -bit ADCs for all RF chains for the AltMin-BF design and set  $b_{\text{total}} = N_r b$  for the GPOS-BFBA scheme. As such, the former represents the proposed beamforming with equal bit allocation, while the latter indicates the proposed joint beamforming and bit allocation with the same total active ADC bits. Furthermore, we include the optimal full-resolution scheme and refer it to “UqOpt”.

### A. Performance Evaluation

In Fig. 2, we show the convergence of the proposed algorithms with  $N_r = N_t = 64$ ,  $N_s = 8$ , SNR = 10 dB,  $b = 2$ ,  $b_{\text{max}} = 8$ , and  $\varsigma = 1$ . It is observed that the GPOS-BFBA algorithm can converge with ten iterations, whereas the AltMin-BF algorithm requires more than 200 iterations for convergence. However, the fewer iterations of the former do not imply a shorter runtime. This is because that each iteration of Algorithm 2 requires running multiple times of Algorithm 1 to evaluate the “quality” of the neighbor points. Nonetheless, the fast convergence of the GPOS-BFBA design shows its efficiency, as seen in the figure that the GPOS-BFBA design achieves a significantly higher SE than the AltMin-BF scheme. We will illustrate this in more detail below.

While the diagonal approximation of  $\mathbf{C}_\eta$  in (40) facilitates the beamformer design and SE maximization, it neglects the off-diagonal entries, which represent the cross-correlation of the signal quantization across the RF chains, inevitably causing SE overestimation. To verify the effectiveness of the proposed designs, in Figs. 3(a) and 3(b), we plot the SE based on both the simulated  $\mathbf{C}_\eta$  and the approximated one (40) versus  $N_r$  with  $N_t = 64$ ,  $N_s = 8$ ,  $b_{\text{max}} = 8$ , and  $\varsigma = 1$ . To



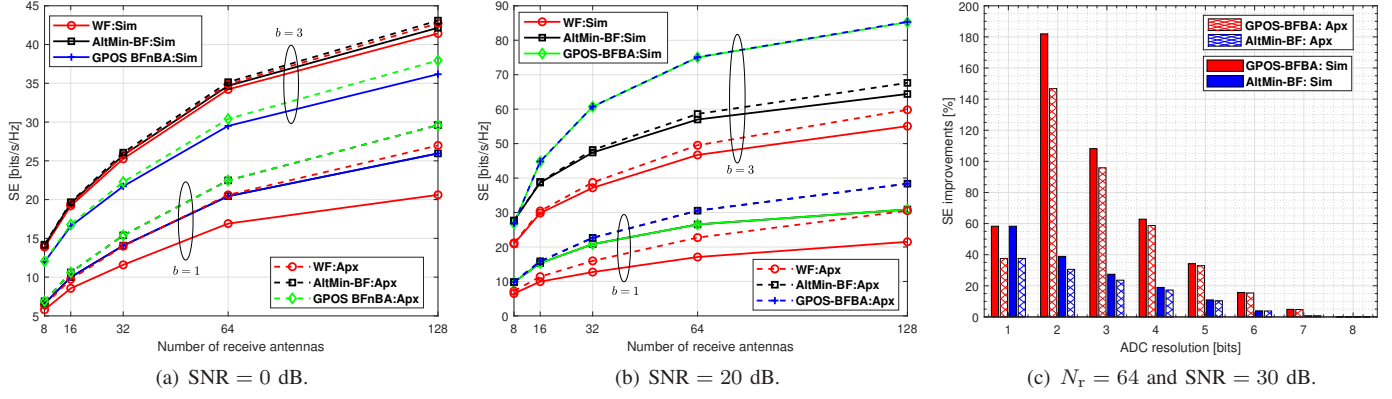


Fig. 3. SE performance with  $N_t = 64$ ,  $N_s = 8$ ,  $b_{\max} = 8$ , and  $\zeta = 1$ . Figs. (a) and (b) show the SE versus the number of receive antennas ( $N_r$ ), while Fig. (c) shows SE improvements relative to the WF scheme versus ADC resolution ( $b$ ).

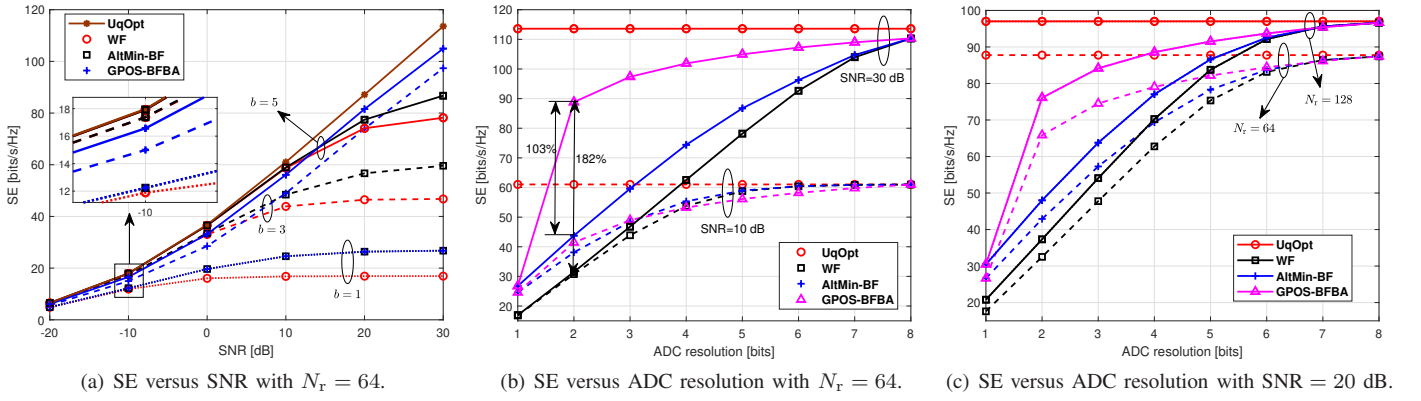


Fig. 4. SE performance with  $N_t = 64$ ,  $N_s = 8$ ,  $b_{\max} = 8$ , and  $\zeta = 1$ .

obtain the simulated  $\mathbf{C}_\eta$ , we randomly generate  $10^5$  Gaussian signal vectors for transmission and determine the optimal quantization of the received signals based on Lemma 2. This process yields  $10^5$  sample variances of the quantization distortion. By averaging these sample variances, we obtain the simulated  $\mathbf{C}_\eta$ . In the figures, the terms ‘‘Sim’’ and ‘‘Apx’’ respectively refer to the SE obtained with the simulated and approximated  $\mathbf{C}_\eta$ . As expected, we can observe that the SE based on the approximated  $\mathbf{C}_\eta$  is much higher than that based on the simulated one. Furthermore, the SE overestimation is more pronounced in systems with higher  $N_r$  and lower-resolution ADCs at high SNR. This is because more receive antennas and lower resolution ADCs increase the number of the cross-correlation term (i.e., the off-diagonal entries) in  $\mathbf{C}_\eta$ , while the low Gaussian noise makes the quantization distortion more significant. Nonetheless, whether the SE is based on the simulated  $\mathbf{C}_\eta$  or the approximated one, the proposed AltMin-BF design significantly outperforms the WF scheme and performs worse than the GPOS-BFBA design with more receive antennas and lower-resolution ADCs at high SNR, as further demonstrated in Fig. 3(c).

In Fig. 3(c), we show the SE improvements achieved by the AltMin-BF and GPOS-BFBA designs relative to the WF scheme versus the ADC resolution with  $N_t = N_r = 64$ ,

$N_s = 8$ ,  $b_{\max} = 8$ , and  $\zeta = 1$ . It is clear that, regardless of whether SE is evaluated based on the simulated  $\mathbf{C}_\eta$  or the approximated one, the proposed AltMin-BF and GPOS-BFBA designs significantly outperform the WF scheme, particularly for lower-resolution systems. Notably, compared to the SE evaluated based on the approximated  $\mathbf{C}_\eta$ , both the GPOS-BFBA and AltMin-BF designs achieve more SE improvements when the SE is evaluated based on the simulated  $\mathbf{C}_\eta$ . Furthermore, the proposed joint beamforming and bit allocation design significantly outperforms the beamforming alone, except for  $b = 1$  where there is no bit allocation. This validates the effectiveness of our proposed designs. Therefore, in the subsequent figures, we only present the performance based on the simulated  $\mathbf{C}_\eta$ .

Fig. 4(a) shows the SE performance versus the SNR with  $N_r = N_t = 64$ ,  $N_s = 8$ ,  $b_{\max} = 8$ ,  $\zeta = 1$ , and  $b \in \{1, 3, 5\}$ . It is observed that the SE achieved by beamforming alone saturates at high SNR due to quantization distortion. Increasing ADC resolution enhances SE, as seen from  $b = 1$  to  $b = 3$ , requiring higher SNR for saturation. For instance, the WF scheme achieves a maximum SE of 16.81 bits/s/Hz at 10 dB with  $b = 1$ , while it is 46.47 bits/s/Hz at 20 dB with  $b = 3$ . The AltMin-BF design shows similar trends, but achieving higher SE at higher SNR. This tendency occurs because in low-

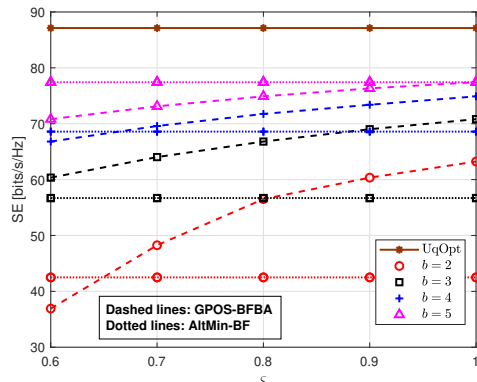
resolution systems, SE saturates when quantization distortion surpasses Gaussian noise, becoming the dominant factor that limits the SE upper bound. Higher ADC resolution reduces this distortion, necessitating higher SNR for SE saturation. However, the proposed GPOS-BFBA design with  $b = 3$  reaches 86% SE of the optimal full-precision system at 30 dB, avoiding saturation for  $b \in \{3, 5\}$  due to the existence of high-resolution ADCs. At low SNR, GPOS-BFBA performs worse than beamforming alone, as also observed in Fig. 3(a), due to significant Gaussian noise. We note that the GPOS-BFBA design with  $b = 1$  reduces to the AltMin-BF scheme since there is no bit allocation.

Fig. 4(b) shows the SE performance versus the ADC resolution with  $N_r = N_t = 64$ ,  $N_s = 8$ ,  $b_{\max} = 8$ ,  $\zeta = 1$ , and  $\text{SNR} \in \{10, 30\}$  dB. We can observe that the SE gradually increases with the ADC resolution until reaching the maximum level limited by the SNR. Furthermore, at a higher SNR, the SE enhancements due to increasing the ADC resolution are more significant, and more ADC bits are required to reach the SE upper bound. For example, at  $\text{SNR} = 10$  dB, 6-bit ADCs are sufficient, while high-resolution (more than 8 bits) ADCs are required at  $\text{SNR} = 30$  dB. This is because a higher SNR makes the quantization distortion more significant, and thereby an increased ADC resolution is necessary for SE to saturate again. Moreover, it is shown the AltMin-BF and GPOS-BFBA designs perform better for low-resolution systems at high SNR. At  $\text{SNR} = 30$  dB, the GPOS-BFBA design with  $b = 2$  attains a 103% and 182% SE improvements compared to the AltMin-BF and WF designs, respectively. Furthermore, with more receive antennas, the SE improvements are more significant, as shown in Fig. 4(c). We can observe that at  $\text{SNR} = 20$  dB, the 8-bit ADCs are sufficient to achieve the optimal SE.

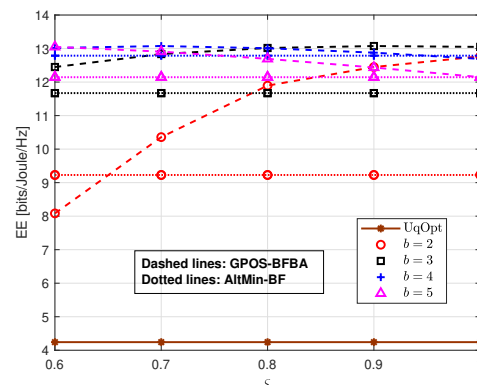
### B. SE and EE tradeoff

We herein characterize the SE–EE tradeoff of the considered system. The EE is defined as the ratio between the SE and the total power consumption of the receiver [7], [47]. The total power consumption of the receiver is given by  $P_{\text{total}} = N_r (P_{\text{LNA}} + P_{\text{RF}} + 2P_{\text{ADC}})$  where  $P_{\text{LNA}}$ ,  $P_{\text{RF}}$ , and  $P_{\text{ADC}}$  denote the power consumption of a low noise amplifier (LNA), an RF chain, and an ADC, respectively. In the following simulations, we set  $P_{\text{RF}} = 43$  mW [7] and  $P_{\text{LNA}} = 25$  mW [48]. Furthermore, a  $b$ -bit ADC typically has a power consumption of  $P_{\text{ADC}} = \kappa f_s 2^b$  [49] where  $\kappa$  and  $f_s$  represent the figure of merit (FoM) and the sampling frequency (ideally equal to signal bandwidth), respectively. In the simulations, we choose a conservative value of the FoM, i.e.,  $\kappa = 494$  fJ/step/Hz [47], for evaluation considering that practical implementations have more limitations than theoretical analysis. Since beamforming alone with few-bit ADCs is sufficient for SE saturation at low SNR, as seen from Figs. 4(a), we only consider the high SNR scenarios in the following.

In Figs. 5(a) and 5(b), we plot the SE and EE of the AltMin-BF and GPOS-BFBA designs as functions of  $\zeta$  with  $N_t = N_r = 64$ ,  $N_s = 8$ ,  $\text{SNR} = 20$  dB, and  $b_{\max} = 5$ . We can observe that the joint beamforming and bit allocation



(a) SE versus  $\zeta$ .



(b) EE versus  $\zeta$ .

Fig. 5. SE and EE versus  $\zeta$  with  $N_t = N_r = 64$ ,  $N_s = 8$ ,  $\text{SNR} = 20$  dB, and  $b_{\max} = 5$ .

design can significantly outperform the beamforming alone in terms of both SE and EE for low-resolution (2–4 bits) systems. Particularly, the GPOS-BFBA design with  $b = 3$  using only 60% of the total bits, can achieve approximately 6% improvements in both SE and EE compared to the AltMin-BF design, which uses 100% of the total bits. Furthermore, the former with  $b = 2$  achieves improvements in 49% SE and 39% EE compared to the latter when  $\zeta = 1$ . For the case  $b = 4$ , GPOS-BFBA design achieves significantly higher SE and comparable EE than that with  $b = 3$  but significantly higher EE than that with  $b = 2$ . Additionally, while the full-precision system achieves significantly higher SE than low-resolution ones, the latter attains substantially higher EE. For example, the GPOS-BFBA design with  $b = 3$  and  $\zeta = 1$  achieves 82% of the optimal SE with a 209% improvement in EE compared to the full-precision system.

Figs. 6(a)–6(c) show the SE and EE of the considered schemes versus the ADC resolution with  $N_t = N_r = 64$ ,  $\text{SNR} = 20$  dB, and  $\zeta = 1$ . Here, we set  $b_{\max} = 5$  for  $b \in \{2, 3, 4\}$  and  $b_{\max} = b + 1$  for  $b \in \{5, 6, 7\}$ . It is observed from Fig. 6(a) that with more data streams, the AltMin-BF design provides more SE improvements compared to the WF scheme. Furthermore, it attains both lower SE and EE compared to the GPOS-BFBA design in low-resolution (2–4 bits) systems, as seen in Fig. 6(b). We can observe that receiving more data streams with low-resolution ADCs can

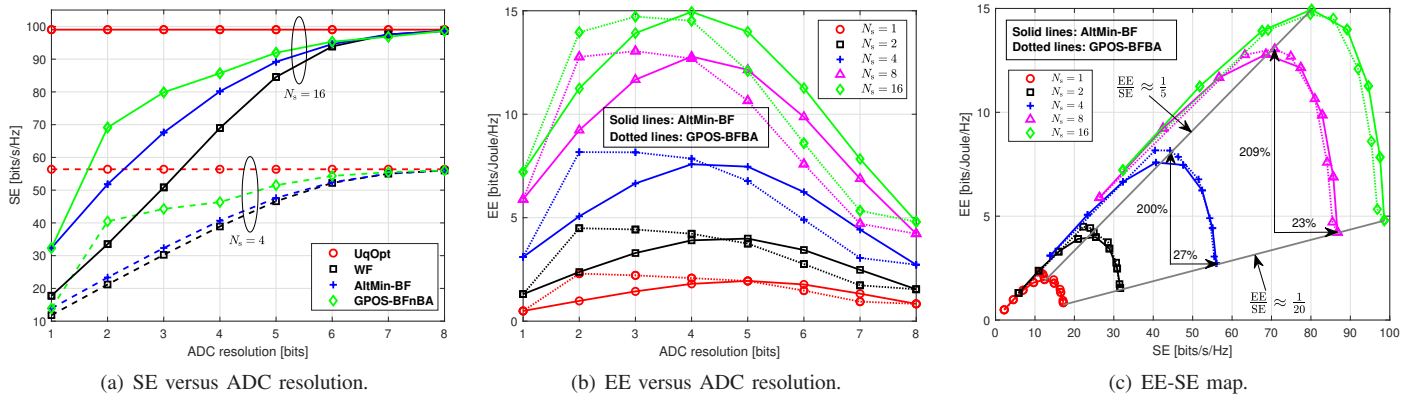


Fig. 6. SE and EE performance versus ADC resolution (b) with  $N_t = N_r = 64$ , SNR = 20 dB, and  $\zeta = 1$ . We set  $b_{\max} = 5$  for  $b \in \{2, 3, 4\}$  and  $b_{\max} = b + 1$  for  $b \in \{5, 6, 7\}$ . The parabolic shape of each line in Fig. (c) is due to the increase of the ADC bit ranging from 1 to 8.

achieve higher SE and EE than receiving fewer data streams with high-resolution ADCs. For example, with  $N_s = 4$  and  $b = 8$ , the SE and EE attained by the AltMin-BF design are 56.01 bits/s/Hz and 2.73 bits/Joule/Hz while their values are 56.09 bits/s/Hz and 11.67 bits/Joule/Hz with  $N_s = 8$  and  $b = 3$ . Finally, we plot the EE-SE map in Fig. 6(c). It is clear that more data streams bring forth both higher EE and higher SE. Moreover, low-resolution systems that sacrifice less than 30% SE can improve more than 200% EE compared to the full-precision ones. Particularly, the EE-SE ratios for low-resolution and full-precision systems are approximately  $\frac{1}{5}$  and  $\frac{1}{20}$ , respectively. Therefore, the former can achieve an approximately fourfold improvement in EE compared to the latter for each unit increase in SE.

## VI. CONCLUSIONS

We have identified the critical properties of optimal quantization, as outlined in Lemma 2 and Lemma 3. We further leveraged these properties to establish the BAQNM and the diagonal approximation of the QD covariance matrix. Our analytical results reveal that the BAQNM and the approximation of the QD covariance typically hold under the premise of Gaussian signaling undergoing optimal quantization, a fact not well recognized in the literature. Additionally, we examine the nuances and connections between applying BAQNM and the arcsine law to one-bit quantization. The consistency of the results obtained from these two methods validates our findings. These findings facilitate the joint design of transmit-receive beamforming and bit allocation in point-to-point MIMO systems with low-resolution ADCs. We first propose an efficient beamforming design for any bit allocation strategy. Building on this, we design a low-complexity joint beamforming design and bit allocation algorithm that iteratively optimizes bit allocation and beamforming matrices.

The numerical simulations show that the proposed designs achieve more SE improvements when the SE is evaluated using the simulated QD covariance rather than the approximated one. The result verifies the effectiveness of the proposed designs. Particularly, the proposed beamforming design significantly outperforms conventional WF solutions for low-resolution

systems, especially for the one-bit case at high SNR. At low SNR, beamforming with equal bit allocation and few-bit (e.g., 3-bit) ADCs is sufficient for SE saturation, whereas higher-resolution ADCs are needed at higher SNR. Moreover, at high SNR, the proposed joint beamforming and bit allocation design with fewer total ADC bits can achieve both higher SE and EE compared to beamforming alone, especially for low-resolution (2–4 bits) systems. Notably, low-resolution systems result in less than 30% SE reduction but can improve EE by more than 200% compared to full-precision ones. In particular, the former can achieve an approximately fourfold improvement in EE compared to the latter for each unit increase in SE. Furthermore, the results demonstrate that receiving more data streams with low-resolution ADCs can yield higher SE and EE than receiving fewer data streams with high-resolution ADCs. Future work may explore system performance with imperfect CSI and compare fully digital architectures with hybrid ones. Moreover, a more accurate quantization modeling for modulated signals in low-resolution systems requires further investigation.

## APPENDIX A

### PROOF FOR LEMMA 2

Denote by  $\{t_j^y, j = 0, \dots, N_q\}$  and  $\{c_j^y, j = 0, \dots, N_q - 1\}$  the thresholds and codebook of the optimal quantizer for  $Y$ , respectively. The MSE between  $Y$  and its optimal quantization  $Q_Y(Y)$  is given by

$$D_Y = \mathbb{E} \left[ (Q_Y(Y) - Y)^2 \right] = \sum_{i=0}^{N_q-1} \int_{t_i^y}^{t_{i+1}^y} (y - c_i^y)^2 f_Y(y) dy$$

$$\stackrel{(a)}{=} \sigma_Y^2 \sum_{i=0}^{N_q-1} \int_{\frac{t_i^y}{\sigma_Y}}^{\frac{t_{i+1}^y}{\sigma_Y}} \left( x - \frac{c_i^y}{\sigma_Y} \right)^2 f_X(x) dx, \quad (54)$$

where (a) is due to  $f_Y(y) = \frac{1}{\sigma_Y} f_X(\frac{y}{\sigma_Y})$ . On the other hand, the thresholds and codebook of the optimal quantizer for  $X$  are respectively denoted by  $\{t_j^x, j = 0, \dots, N_q\}$  and  $\{c_j^x, j = 0, \dots, N_q - 1\}$ . These minimize the quantization MSE of  $X$ , i.e.,

$$D_X = \mathbb{E} \left[ (Q_X(X) - X)^2 \right] = \sum_{i=0}^{N_q-1} \int_{t_i^x}^{t_{i+1}^x} (x - c_i^x)^2 f_X(x) dx. \quad (55)$$

Therefore, with  $c_i^y = \sigma_y c_i^x$ , which leads to  $t_i^y = \sigma_y t_i^x$  (due to condition (12)),  $D_y$  is minimized and satisfies  $D_y = \sigma_y^2 D_x$ . These result in (15) and (16) in Lemma 2.

#### APPENDIX B PROOF FOR LEMMA 3

For a real zero-mean random variable  $Y$ , let  $Q(Y)$  denote the output of the Lloyd-Max quantizer. The centroid condition (13) implies [35, Chapter 6]:

$$\mathbb{E}[Q(Y)] = \mathbb{E}[Y], \quad (56)$$

$$\mathbb{E}[Q(Y)(Q(Y) - Y)] = 0. \quad (57)$$

Hence, for  $X = \Re\{X\} + j\Im\{X\}$ , we have

$$\mathbb{E}[Q(X)] = \mathbb{E}[Q(\Re\{X\})] + j\mathbb{E}[Q(\Im\{X\})] = \mathbb{E}[X]. \quad (58)$$

With  $\chi \triangleq Q(X) - X$ , we can obtain

$$\mathbb{E}[Q(X)\chi^*] = \mathbb{E}[Q(X)(Q(X) - X)^*] = 0, \quad (59)$$

where the last equality follows (57) and the assumption that  $\Re\{X\}$  and  $\Im\{X\}$  are i.i.d and independently quantized. Because  $\Re\{X\}$  and  $\Im\{X\}$  have the same variance of  $\sigma_X^2/2$ , we have

$$\mathbb{E}[|X|^2] = 2\mathbb{E}[\Re\{X\}^2] = 2\mathbb{E}[\Im\{X\}^2], \quad (60)$$

$$\mathbb{E}[|\chi|^2] = 2\mathbb{E}[\Re\{\chi\}^2] = 2\mathbb{E}[\Im\{\chi\}^2], \quad (61)$$

yielding the distortion factor

$$\gamma = \frac{\mathbb{E}[|\chi|^2]}{\mathbb{E}[|X|^2]} = \frac{\mathbb{E}[\Re\{\chi\}^2]}{\mathbb{E}[\Re\{X\}^2]} = \frac{\mathbb{E}[\Im\{\chi\}^2]}{\mathbb{E}[\Im\{X\}^2]} \quad (62)$$

in Lemma 3.

#### APPENDIX C PROOF FOR LEMMA 5

The quantization error  $q_m = z_m - y_m$ , conditioned on  $y_m$ , is statistically independent of all other random variables of the system. Hence, for  $m \neq n$ , we have

$$\begin{aligned} \mathbb{E}[q_m q_n^*] &= \mathbb{E}[\mathbb{E}[q_m q_n^* | y_n]] = \mathbb{E}[\mathbb{E}[q_m | y_n] \mathbb{E}[q_n^* | y_n]] \\ &\stackrel{(a)}{\approx} \mathbb{E}[C_{q_m, y_n} C_{y_n}^{-1} y_n \mathbb{E}[q_n^* | y_n]] = C_{q_m, y_n} C_{y_n}^{-1} \mathbb{E}[y_n q_n^*], \end{aligned} \quad (63)$$

where (a) is due to the LMMSE estimation. Furthermore, we have

$$\begin{aligned} C_{q_m, y_n} &= \mathbb{E}[q_m y_n^*] = \mathbb{E}[(z_m - y_m) y_n^*] = C_{z_m, y_n} - C_{y_m, y_n} \\ &\stackrel{(c)}{=} (g_m - 1) C_{y_m, y_n} \stackrel{(d)}{=} -\gamma_m C_{y_m, y_n}, \end{aligned} \quad (64)$$

where (c) and (d) are due to Lemmas 1 and 4, respectively. Similarly, we obtain

$$\begin{aligned} \mathbb{E}[y_n q_m^*] &= \mathbb{E}[y_n (z_m - y_m)^*] = C_{z_n, y_n}^* - C_{y_n} \\ &= C_{y_n} (g_n^* - 1) = -\gamma_n C_{y_n}. \end{aligned} \quad (65)$$

Based on (63)–(65), we obtain  $\mathbb{E}[q_m q_n^*] \approx \gamma_m \gamma_n \mathbb{E}[y_m y_n^*]$ . Combined with  $\mathbb{E}[q_n q_n^*] = \gamma_n \mathbb{E}[y_n y_n^*]$ , we have

$$\begin{aligned} \mathbf{C}_q &\approx \text{diag}(\mathbf{C}_y) \mathbf{\Gamma} + \mathbf{\Gamma} \text{nondiag}(\mathbf{C}_y) \mathbf{\Gamma} \\ &= \mathbf{\Gamma} \mathbf{C}_y \mathbf{\Gamma} + (\mathbf{I} - \mathbf{\Gamma}) \text{diag}(\mathbf{C}_y) \mathbf{\Gamma}, \end{aligned} \quad (66)$$

where  $\text{nondiag}(\mathbf{A})$  denotes the matrix containing all non-diagonal entries of  $\mathbf{A}$  while its diagonal entries are all zero. Based on (27) and (28), we have

$$\mathbf{C}_\eta \approx \mathbf{\Gamma} \text{diag}(\mathbf{C}_y) (\mathbf{I} - \mathbf{\Gamma}), \quad (67)$$

$$\mathbf{C}_z \approx [\text{diag}(\mathbf{C}_y) \mathbf{\Gamma} + (\mathbf{I} - \mathbf{\Gamma}) \mathbf{C}_y] (\mathbf{I} - \mathbf{\Gamma}). \quad (68)$$

It is observed from the results  $\mathbb{E}[q_m q_n^*] \approx \gamma_m \gamma_n \mathbb{E}[y_m y_n^*]$  and  $\mathbb{E}[q_n q_n^*] = \gamma_n \mathbb{E}[y_n y_n^*]$  that the cross-correlation coefficient is obtained by the LMMSE estimation while the auto-correlation coefficient comes from the definition of distortion factor. Therefore, the diagonal entries of  $\mathbf{C}_\eta$  are exactly the ones of  $\mathbf{\Gamma} \text{diag}(\mathbf{C}_y) (\mathbf{I} - \mathbf{\Gamma})$ . As such, the approximation is due to neglecting the non-zero off-diagonal entries of  $\mathbf{C}_\eta$ .

#### APPENDIX D PROOF FOR PROPOSITION 1

With the first-order condition of local optima, we obtain

$$\mathbf{W} = \mathbf{E}^{-1}, \quad (69)$$

$$\mathbf{U} = (\mathbf{G} \mathbf{H} \mathbf{F} \mathbf{F}^H \mathbf{H}^H \mathbf{G} + \mathbf{C}_e)^{-1} \mathbf{G} \mathbf{H} \mathbf{F}. \quad (70)$$

Therefore, the MSE matrix can be recast as

$$\mathbf{E} = \mathbf{I} - \mathbf{F}^H \mathbf{H}^H \mathbf{G} (\mathbf{G} \mathbf{H} \mathbf{F} \mathbf{F}^H \mathbf{H}^H \mathbf{G} + \mathbf{C}_e)^{-1} \mathbf{G} \mathbf{H} \mathbf{F}. \quad (71)$$

Using the Woodbury matrix identity, we obtain

$$\mathbf{E}^{-1} = \mathbf{I} + \mathbf{F}^H \mathbf{H}^H \mathbf{G} \mathbf{C}_e^{-1} \mathbf{G} \mathbf{H} \mathbf{F} = \mathbf{W}. \quad (72)$$

Therefore, we have

$$\begin{aligned} f(\mathbf{U}, \mathbf{F}, \mathbf{W}) &= N_t - \log \det(\mathbf{E}^{-1}) \\ &= N_t - \log \det(\mathbf{I} + \mathbf{C}_e^{-1} \mathbf{G} \mathbf{H} \mathbf{F} \mathbf{F}^H \mathbf{H}^H \mathbf{G}). \end{aligned} \quad (73)$$

We next show that  $R = \det(\mathbf{I} + \mathbf{C}_e^{-1} \mathbf{G} \mathbf{H} \mathbf{F} \mathbf{F}^H \mathbf{H}^H \mathbf{G})$  with  $\mathbf{U}$  given by the MMSE solution (70). With  $\mathbf{L} \triangleq \mathbf{G} \mathbf{H} \mathbf{F}$ ,  $\mathbf{U}$  can be written as  $\mathbf{U} = (\mathbf{L} \mathbf{L}^H + \mathbf{C}_e)^{-1} \mathbf{L}$  based on (70). Furthermore, by the Woodbury matrix identity, we obtain

$$\mathbf{U} = \mathbf{C}_e^{-1} \mathbf{L} - \mathbf{C}_e^{-1} \mathbf{L} (\mathbf{I} + \mathbf{L}^H \mathbf{C}_e^{-1} \mathbf{L})^{-1} \mathbf{L}^H \mathbf{C}_e^{-1} \mathbf{L}, \quad (74)$$

which results in

$$\mathbf{U}^H \mathbf{C}_e = (\mathbf{I} - \mathbf{P} (\mathbf{I} + \mathbf{P}))^{-1} \mathbf{L}^H \mathbf{U} = (\mathbf{I} + \mathbf{P})^{-1} \mathbf{L}^H \mathbf{U}, \quad (75a)$$

$$\mathbf{L}^H \mathbf{U} = \mathbf{P} (\mathbf{I} - \mathbf{P} (\mathbf{I} + \mathbf{P})^{-1}) = \mathbf{P} (\mathbf{I} + \mathbf{P})^{-1}, \quad (75b)$$

where  $\mathbf{P} \triangleq \mathbf{L}^H \mathbf{C}_e^{-1} \mathbf{L}$  and we note that  $(\mathbf{I} + \mathbf{P})^{-1} = \mathbf{I} - (\mathbf{I} + \mathbf{P})^{-1} \mathbf{P} = \mathbf{I} - \mathbf{P} (\mathbf{I} + \mathbf{P})^{-1}$ . With (75), we derive

$$\begin{aligned} R &= \log \det(\mathbf{I} + (\mathbf{U}^H \mathbf{C}_e \mathbf{U})^{-1} \mathbf{U}^H \mathbf{L} \mathbf{L}^H \mathbf{U}) = \log \det(\mathbf{I} + \mathbf{P}) \\ &= \log \det(\mathbf{I} + \mathbf{C}_e^{-1} \mathbf{G} \mathbf{H} \mathbf{F} \mathbf{F}^H \mathbf{H}^H \mathbf{G}) \\ &= N_t - f(\mathbf{U}, \mathbf{F}, \mathbf{W}). \end{aligned} \quad (76)$$

Hence, problem (45) is equivalent to (43) when  $\mathbf{U}$  and  $\mathbf{W}$  are given by (47) and (46), respectively.

#### REFERENCES

- [1] R. W. Heath, N. Gonzalez-Prelcic, S. Rangan, W. Roh, and A. M. Sayeed, "An overview of signal processing techniques for millimeter wave MIMO systems," *IEEE J. Sel. Areas Commun.*, vol. 10, no. 3, pp. 436–453, 2016.
- [2] W. Jiang, B. Han, M. A. Habibi, and H. D. Schotten, "The road towards 6G: A comprehensive survey," *IEEE Open J. Commun. Soc.*, vol. 2, pp. 334–366, 2021.
- [3] Y. Li, C. Tao, G. Seco-Granados, A. Mezghani, A. L. Swindlehurst, and L. Liu, "Channel estimation and performance analysis of one-bit massive MIMO systems," *IEEE Trans. Signal Process.*, vol. 65, no. 15, pp. 4075–4089, 2017.

- [4] B. Murmann, "The race for the extra decibel: A brief review of current ADC performance trajectories," *IEEE Solid-State Circuits Mag.*, vol. 7, no. 3, pp. 58–66, 2015.
- [5] I. Atzeni, A. Töllli, and G. Durisi, "Low-resolution massive MIMO under hardware power consumption constraints," in *Proc. Asilomar Conf. Signals, Syst., Comp.*, 2021.
- [6] J. Liu, Z. Luo, and X. Xiong, "Low-resolution ADCs for wireless communication: A comprehensive survey," *IEEE Access*, vol. 7, pp. 91 291–91 324, 2019.
- [7] R. Méndez-Rial, C. Rusu, N. González-Prelcic, A. Alkhateeb, and R. W. Heath, "Hybrid MIMO architectures for millimeter wave communications: Phase shifters or switches?" *IEEE Access*, vol. 4, pp. 247–267, 2016.
- [8] M. Ma, N. T. Nguyen, and M. Juntti, "Closed-form hybrid beamforming solution for spectral efficiency upper bound maximization in mmWave MIMO-OFDM systems," in *Proc. IEEE Veh. Technol. Conf.*, 2021.
- [9] —, "Switch-based hybrid beamforming transceiver design for wideband communications with beam squint," *arXiv preprint arXiv:2210.06890*, 2022.
- [10] K. Roth, H. Pirzadeh, A. L. Swindlehurst, and J. A. Nossek, "A comparison of hybrid beamforming and digital beamforming with low-resolution ADCs for multiple users and imperfect CSI," *IEEE J. Sel. Topics Signal Process.*, vol. 12, no. 3, pp. 484–498, 2018.
- [11] H. Yan, S. Ramesh, T. Gallagher, C. Ling, and D. Cabric, "Performance, power, and area design trade-offs in millimeter-wave transmitter beamforming architectures," *IEEE Circuits Syst. Mag.*, vol. 19, no. 2, pp. 33–58, 2019.
- [12] O. Castañeda, Z. Boynton, S. H. Mirfarshbafan, S. Huang, C. Y. Jamie, A. Molnar, and C. Studer, "A resolution-adaptive 8 mm<sup>2</sup> 9.98 Gb/s 39.7 pJ/b 32-antenna all-digital spatial equalizer for mmWave massive MU-MIMO in 65nm CMOS," in *Proc. Solid-State Circ. Conf.*, 2021.
- [13] D. Tse and P. Viswanath, *Fundamentals of wireless communication*. Cambridge university press, 2005.
- [14] O. Castañeda, S. H. Mirfarshbafan, S. Ghajari, A. Molnar, S. Jacobsson, G. Durisi, and C. Studer, "Resolution-adaptive all-digital spatial equalization for mmWave massive MU-MIMO," in *Proc. IEEE Workshop Signal Proc. Adv. in Wirel. Comms.*, 2021.
- [15] J. Singh, O. Dabeer, and U. Madhow, "On the limits of communication with low-precision analog-to-digital conversion at the receiver," *IEEE Trans. Commun.*, vol. 57, no. 12, pp. 3629–3639, 2009.
- [16] J. Mo and R. W. Heath, "Capacity analysis of one-bit quantized MIMO systems with transmitter channel state information," *IEEE Trans. Signal Process.*, vol. 63, no. 20, pp. 5498–5512, 2015.
- [17] A. Mezghani and J. A. Nossek, "Analysis of rayleigh-fading channels with 1-bit quantized output," in *Proc. IEEE Int. Symp. Inf. Theory*, 2008.
- [18] —, "On ultra-wideband MIMO systems with 1-bit quantized outputs: Performance analysis and input optimization," in *Proc. IEEE Int. Symp. Inf. Theory*, 2007.
- [19] I. Atzeni and A. Töllli, "Channel estimation and data detection analysis of massive MIMO with 1-bit ADCs," *IEEE Trans. Wireless Commun.*, vol. 21, no. 6, pp. 3850–3867, 2021.
- [20] O. Orhan, E. Erkip, and S. Rangan, "Low power analog-to-digital conversion in millimeter wave systems: Impact of resolution and bandwidth on performance," in *Proc. ITG Workshop Smart Antennas*, 2015.
- [21] S. Jacobsson, G. Durisi, M. Coldrey, U. Gustavsson, and C. Studer, "Throughput analysis of massive MIMO uplink with low-resolution ADCs," *IEEE Trans. Wireless Commun.*, vol. 16, no. 6, pp. 4038–4051, 2017.
- [22] A. Mezghani and J. A. Nossek, "Capacity lower bound of MIMO channels with output quantization and correlated noise," in *Proc. IEEE Int. Symp. Inf. Theory*, 2012.
- [23] A. Mezghani, R. Ghiat, and J. A. Nossek, "Transmit processing with low resolution D/A-converters," in *Proc. IEEE Int. Conf. Electron., Circuits, Syst.*, 2009.
- [24] S. Jacobsson, G. Durisi, M. Coldrey, T. Goldstein, and C. Studer, "Quantized precoding for massive MU-MIMO," *IEEE Trans. Wireless Commun.*, vol. 65, no. 11, pp. 4670–4684, 2017.
- [25] X. Ling and R. Wang, "Performance analysis and transceiver design of few-bit quantized MIMO systems," *IEEE Access*, vol. 7, pp. 9935–9944, 2019.
- [26] T.-C. Zhang, C.-K. Wen, S. Jin, and T. Jiang, "Mixed-ADC massive MIMO detectors: Performance analysis and design optimization," *IEEE Trans. Wireless Commun.*, vol. 15, no. 11, pp. 7738–7752, 2016.
- [27] J. Zhang, L. Dai, Z. He, S. Jin, and X. Li, "Performance analysis of mixed-ADC massive MIMO systems over Rician fading channels," *IEEE J. Sel. Areas Commun.*, vol. 35, no. 6, pp. 1327–1338, 2017.
- [28] H. Pirzadeh and A. L. Swindlehurst, "Spectral efficiency of mixed-ADC massive MIMO," *IEEE Trans. Signal Process.*, vol. 66, no. 13, pp. 3599–3613, 2018.
- [29] Q. Bai, A. Mezghani, and J. A. Nossek, "On the optimization of ADC resolution in multi-antenna systems," in *Proc. Int. Symp. Wireless Commun. Systems*, 2013.
- [30] I. Z. Ahmed, H. Sadjadpour, and S. Yousefi, "A joint combiner and bit allocation design for massive MIMO using genetic algorithm," in *Proc. Asilomar Conf. Signals, Syst., Comp.*, 2017.
- [31] J. Choi, B. L. Evans, and A. Gatherer, "Resolution-adaptive hybrid MIMO architectures for millimeter wave communications," *IEEE Trans. Signal Process.*, vol. 65, no. 23, pp. 6201–6216, 2017.
- [32] K.-G. Nguyen, Q.-D. Vu, L.-N. Tran, and M. Juntti, "Energy-efficient bit allocation for resolution-adaptive ADC in multiuser large-scale MIMO systems: Global optimality," in *Proc. IEEE Int. Conf. Acoust., Speech, and Signal Process.*, 2020.
- [33] N. Prasad, X. F. Qi, and A. Molev-Shteiman, "Optimizing resolution-adaptive massive MIMO networks," in *Proc. IEEE Int. Conf. on Comp. Commun.*, 2020.
- [34] G. Jacovitti and A. Neri, "Estimation of the autocorrelation function of complex gaussian stationary processes by amplitude clipped signals," *IEEE Trans. Inf. Theory*, vol. 40, no. 1, pp. 239–245, 1994.
- [35] A. Gersho and R. M. Gray, *Vector quantization and signal compression*. Springer Science & Business Media, 2012, vol. 159.
- [36] A. K. Fletcher, S. Rangan, V. K. Goyal, and K. Ramchandran, "Robust predictive quantization: Analysis and design via convex optimization," *IEEE J. Sel. Topics Signal Process.*, vol. 1, no. 4, pp. 618–632, 2007.
- [37] J. J. Bussgang, "Crosscorrelation functions of amplitude-distorted Gaussian signals," Res. Lab. Electron., Massachusetts Inst. Technol., Tech. Rep. 216, 1952.
- [38] S. N. Diggavi and T. M. Cover, "The worst additive noise under a covariance constraint," *IEEE Trans. Inf. Theory*, vol. 47, no. 7, pp. 3072–3081, 2001.
- [39] B. Hassibi and B. M. Hochwald, "How much training is needed in multiple-antenna wireless links?" *IEEE Trans. Inf. Theory*, vol. 49, no. 4, pp. 951–963, 2003.
- [40] O. T. Demir and E. Björnson, "The Bussgang decomposition of nonlinear systems: Basic theory and MIMO extensions [lecture notes]," *IEEE Signal Process. Mag.*, vol. 38, no. 1, pp. 131–136, 2020.
- [41] Y. Wang, X. Chen, Y. Cai, B. Champagne, and L. Hanzo, "Channel estimation for hybrid massive MIMO systems with adaptive-resolution ADCs," *IEEE Trans. Commun.*, vol. 70, no. 3, pp. 2131–2146, 2022.
- [42] E. Björnson, L. Sanguinetti, and J. Hoydis, "Hardware distortion correlation has negligible impact on UL massive MIMO spectral efficiency," *IEEE Trans. Commun.*, vol. 67, no. 2, pp. 1085–1098, 2018.
- [43] J. Max, "Quantizing for minimum distortion," *IRE Trans. Inf. Theory*, vol. 6, no. 1, pp. 7–12, 1960.
- [44] O. B. Usman, H. Jedda, A. Mezghani, and J. A. Nossek, "MMSE precoder for massive MIMO using 1-bit quantization," in *Proc. IEEE Int. Conf. Acoust., Speech, and Signal Process.*, 2016.
- [45] T. S. Rappaport, R. W. Heath Jr, R. C. Daniels, and J. N. Murdock, *Millimeter wave wireless communications*. Pearson Education, 2015.
- [46] X. Yu, J.-C. Shen, J. Zhang, and K. B. Letaief, "Alternating minimization algorithms for hybrid precoding in millimeter wave MIMO systems," *IEEE J. Sel. Topics Signal Process.*, vol. 10, no. 3, pp. 485–500, 2016.
- [47] W. B. Abbas, F. Gomez-Cuba, and M. Zorzi, "Millimeter wave receiver efficiency: A comprehensive comparison of beamforming schemes with low resolution ADCs," *IEEE Trans. Wireless Commun.*, vol. 16, no. 12, pp. 8131–8146, 2017.
- [48] L. Gao and G. M. Rebeiz, "A 22–44-GHz phased-array receive beamformer in 45-nm CMOS SOI for 5G applications with 3–3.6-dB NF," *IEEE Trans. Microw. Theory Techn.*, vol. 68, no. 11, pp. 4765–4774, 2020.
- [49] M. Ma, N. T. Nguyen, I. Atzeni, and M. Juntti, "Analysis of oversampling in uplink massive MIMO-OFDM with low-resolution ADCs," in *Proc. IEEE Workshop Signal Proc. Adv. in Wirel. Comms.*, 2023.